Supplement for

Sources of organic gases and aerosol particles and their roles in nighttime particle growth at a rural forested site in southwest Germany

Junwei Song [1,2, 3], Harald Saathoff [1,3], Feng Jiang [1,2], Linyu Gao [1,2,3], Hengheng Zhang [1] and Thomas Leisner [1]

[1] Institute of Meteorology and Climate Research, Karlsruhe Institute of Technology, Hermann-von-Helmholtz-Platz 1, 76344 Eggenstein-Leopoldshafen, Germany

[2] Institute of Geography and Geoecology, Karlsruhe Institute of Technology, Reinhard-Baumeister-Platz 1, 76131, Karlsruhe, Germany

[3] Now at Univ. Lyon, Université Claude Bernard Lyon 1, CNRS, IRCELYON, 69626 Villeurbanne, France

Text S1. Data processing of CHARON-PTR-MS

The raw data of CHARON-PTR-MS was processed by the Ionicon Data Analyzer (IDA 1.0.2, Ionicon Analytik). Mass calibrations were performed using four ion peaks including $H_3^{18}O^+$ at *m/z* 21.0226, $C_3H_6OH^+$ at *m/z* 59.0491, $C_6H_5I^+$ at *m/z* 203.943 and $C_6H_5I_2^+$ at m/z 330.848, where $C_6H_5I^+$ and $C_6H_5I_2^+$ were produced from the internal standard diiodobenzene. High-resolution peak fitting for each ion was performed automatically by the IDA software and refined manually according to the database of PTR-ToF-MS literature (Pagonis et al., 2019; Yáñez-Serrano et al., 2021). The quantification procedure of CHARON-PTR-MS data has been described in detail by (Muller et al., 2017). The collision rate (k) between the analyte molecules and reagent ions (H_3O^+) is calculated based on the parametrization method (Su, 1988). This method uses the properties of the analyte molecule as input parameters: (i) its molecular weight, (ii) its molecular polarizability which is calculated from the elemental composition using the parametrization method (Bosque and Sales, 2002) and (iii) its dipole moment which is assumed to be 0.3 and 2.75 D for pure and substituted hydrocarbons, respectively. The estimated accuracy of this quantification method is ±30%. Further data analyses including gas and particle data separation, and background subtraction were performed with custom-in MATLAB scripts in IDA. Since the PTR-MS shows slow responses to some organic species especially oxidized species in the particle phase (Piel et al., 2021), the initial 290 s particle-phase data at each CHARON measurement cycle were excluded. Then the processed particle data were corrected by the interpolate subtraction of HEPA filter background. For the gas phase data, we excluded the first 10 s and the last 10 s data at each VOC

measurement cycle to avoid any inferences due to the switching between different measurement modes. Then we subtracted the gas background from the measurement of VOC-free synthetic air. Finally, we averaged the gas and particle phase background-corrected data into 5 min presented in this study.

The PTR-MS suffers the ionic fragmentation during the protonation processes (Yuan et al., 2017). According to gas calibrations, the residual fractions were on average 17% ± 2 % and 37% ± 1 % for protonated isoprene ($C_5H_9^+$, m/z69.07) and monoterpenes ($C_{10}H_{17}^+$, m/z137.13) respectively after their fragmentation within the instrument. Based on the calibration of β-caryophyllene for our instrument in the lab (Gao et al., 2022), we assumed all sesquiterpenes following the similar fragmentation pattern of β-caryophyllene with 29% ± 1 % at protonated sesquiterpene mass ($C_{15}H_{25}^+$, m/z205.20). Finally, we scaled the measured data of $C_5H_9^+$, $C_{10}H_{17}^+$ and $C_{15}H_{25}^+$ for the mixing ratios of isoprene, monoterpenes and sesquiterpenes in this study. For the calibrated aromatic hydrocarbon species (benzene, toluene, xylenes, trimethylbenzene) and acetone, they have minor fragmentation and thus no further correction for their mixing ratios. Besides, no further correction was made for other uncalibrated VOC species.

Text S2. Comparison with the air quality monitor station data

The hourly particle mass and trace gas data (i.e., $PM_{2.5}$, PM_{10}, O_3, NO_2, NO and SO_2) were retrieved from the air quality monitor station of Eggenstein (LUBW), located ~2.5 km southwest of our sampling site (https://udo.lubw.baden-wuerttemberg.de/public/, last access: 1/25/2022). We compared the available data ($PM_{2.5}$, PM_{10}, O_3 and NO_2) at KITcn to those obtained from the Eggenstein monitor station. As shown in Figs. S2 and S3, good correlations were found for the particle mass concentrations measured at these two locations (r = 0.91 for $PM_{2.5}$ and 0.76 for PM_{10}). A good linear correlation was also observed for the O_3 data (r = 0.86), but a poor correlation was found for the NO_2 data (r = 0.27). This is expected due to traffic emissions at Eggenstein station, which could lead to more spikes of NO_2 (Fig. S2). If peak values of NO_2 at the Eggenstein monitor station were removed, a better correlation for NO_2 was observed for both locations (r = 0.64).

Text S3. Estimation of particulate organic nitrate from AMS data

The derived ratio of NO_2^+/NO^+ from AMS data can be used as an indicator for the formation of organic nitrate (Kiendler-Scharr et al., 2016; Xu et al., 2015; Farmer et al., 2010). Here we used the measured NO_2^+/NO^+ ratios to estimate the fraction of organic nitrate ($OrgNO_3$), although this estimation requires accurate ratios for pure ammonium nitrate and organic nitrate. In this study, the average ratio of NO_2^+/NO^+ for calibration using pure ammonium nitrate (NH_4NO_3) three times is 0.61, which is within the ranges (0.29-0.85) reported in previous observations in Europe (Kiendler-Scharr et al., 2016). Based on previous chamber and field studies on organic nitrates, we adopted a fixed value of NO_2^+/NO^+ with 0.1 for organic nitrates (R_{OrgNO3}). The mass fraction and concentration ($pOrgNO3_{Frac}$ and $pOrgNO3_{Mass}$) can be calculated using the following equations:

$$pOrgNO3_{Frac} = \frac{\left(1 + R_{OrgNO3}\right) * (R_{meas} - R_{calib})}{(1 + R_{meas}) * (R_{OrgNO3} - R_{calib})}$$

$$pOrgNO3_{Mass} = pOrgNO3_{Frac} * NO3$$

where R_{meas} is the measured ratios of NO_2^+ and NO^+ ions from AMS data, R_{calib} is the ratio in the calibration of NH_4NO_3. It should be noted that $pOrgNO_3$ calculated from AMS data only indicate the nitrate functional group of organic nitrates. We converted the mass concentrations of $pOrgNO_3$ to $OrgNO_3$ scaled by a factor of 4.2 based on the molecular weight of organic nitrate with 260 g mol^{-1} from the FIGAERO-CIMS measurement.

As shown in Fig. S11, we also observed that $C_{10}H_{15}O_7N$ and $C_{15}H_{23}O_7N$ showed better correlations with the calculated $OrgNO_3$ from the AMS compared to $C_5H_7O_7N$. Note that these three particulate molecules measured by the FIGAERO-CIMS the have been proposed as the major oxidation products of isoprene, monoterpenes and sesquiterpenes respectively with nitrate radicals in the field or chamber studies (Huang et al., 2019; Chen et al., 2020; Gao et al., 2022).
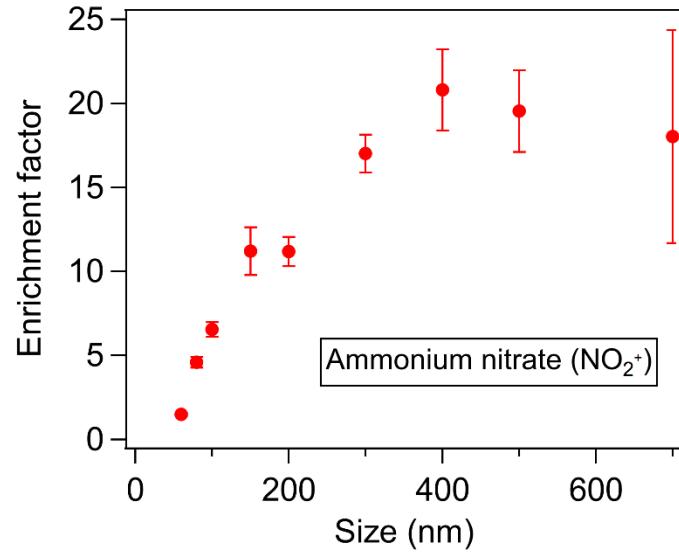
Figure S1. Calibrated enrichment factor of ammonium nitrate particles as a function of particle size in the 60-700 nm range
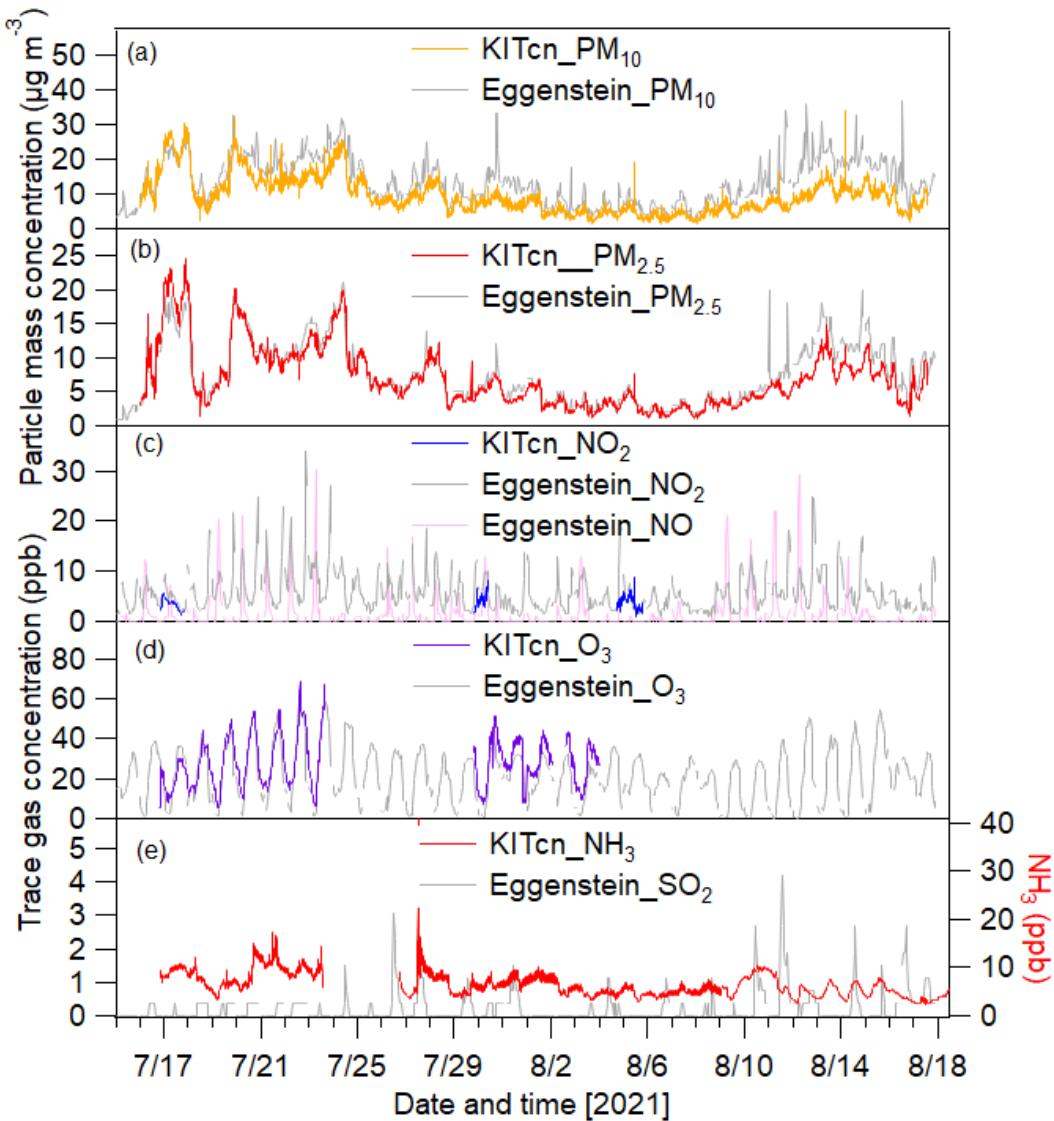
Figure S2. Time series of (a) PM_{10}, (b) $PM_{2.5}$, (c) NO_2 and NO, (d) O_3 and (e) SO_2 and NH_3 observed at the sampling site (KITcn) and Eggenstein air quality monitor station during the measurement period. The trace gas data of NO_2 and O_3 are only available for few days due to malfunction of the data acquisition software.
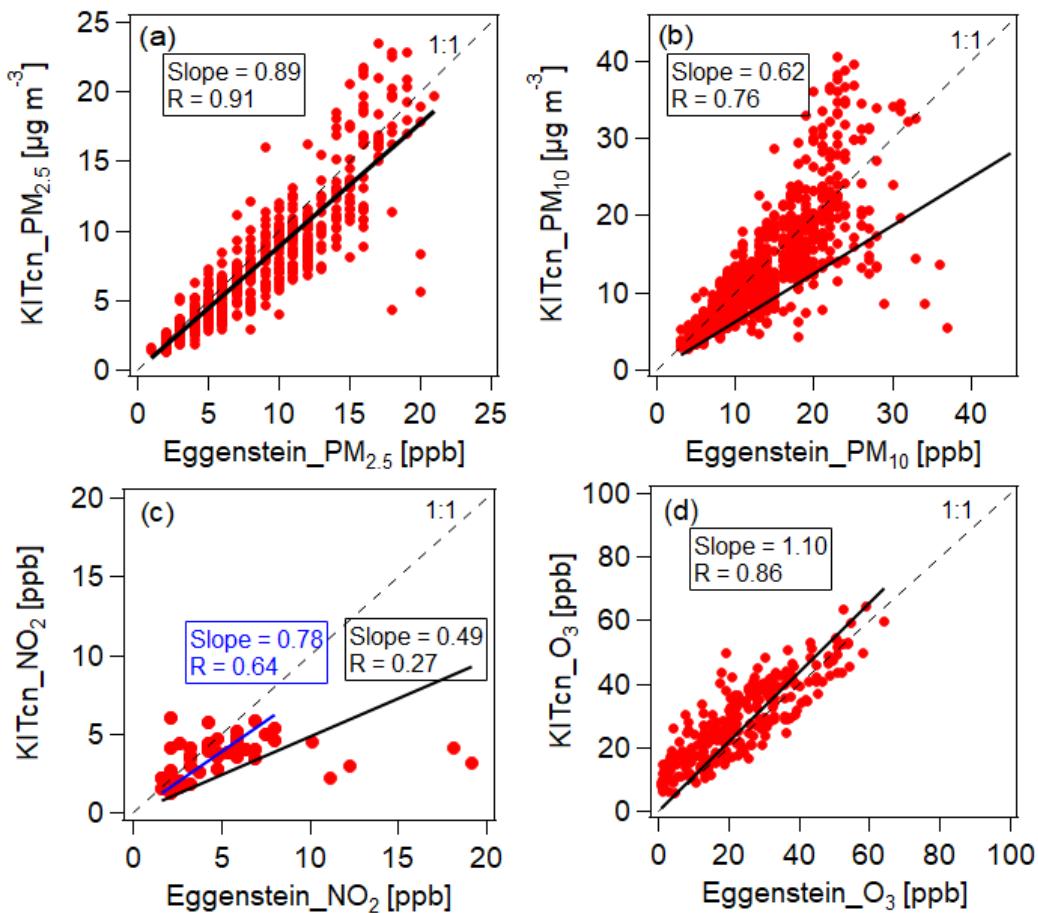
Figure S3. Scatter plots for (a) PM$_{2.5}$, (b) PM$_{10}$, (c) NO$_2$ and (d) O$_3$ measured at the sampling site (KITcn) and Eggenstein air quality monitor station during the measurement period. The black solid and dash lines represent the linear fit curve and 1:1 line, respectively. The blue solid line in (c) shows the linear fit curve after removing high NO$_2$ values (>10 ppb) observed at Eggenstein monitor station.
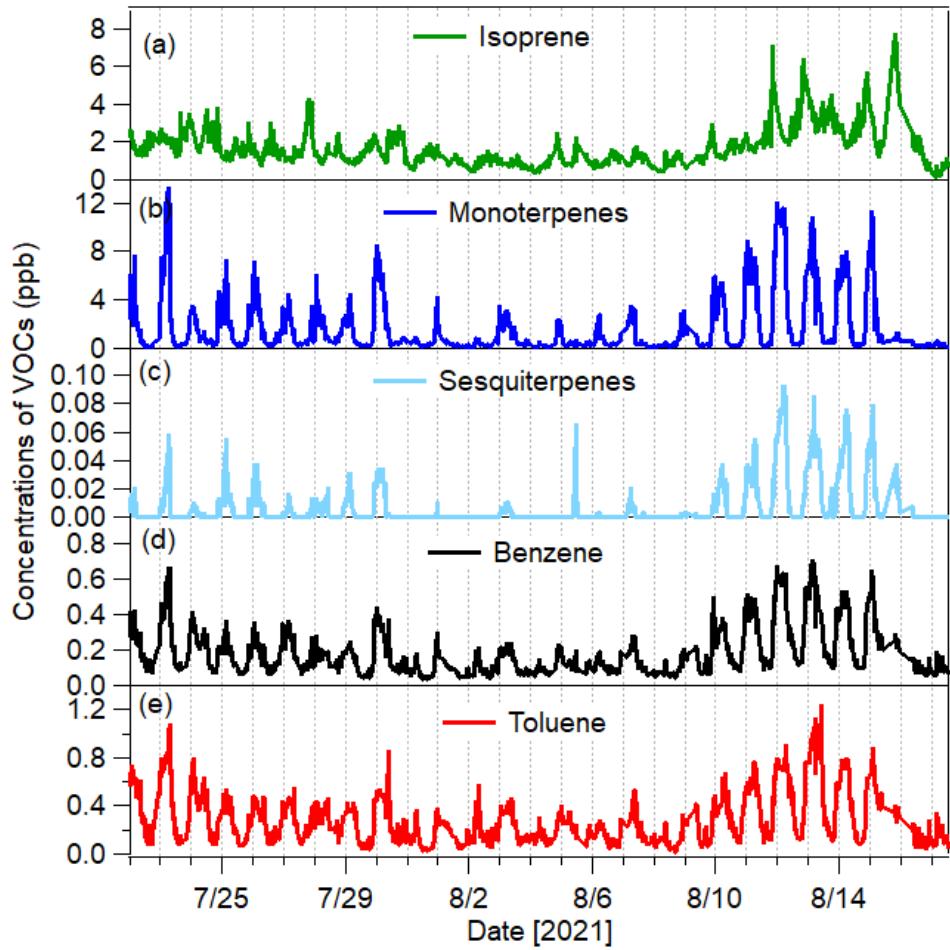
Figure S4. Time series of concentrations of selected VOC species. (a) isoprene; (b) monoterpenes; (c) sesquiterpenes; (d) benzene and (e) toluene.
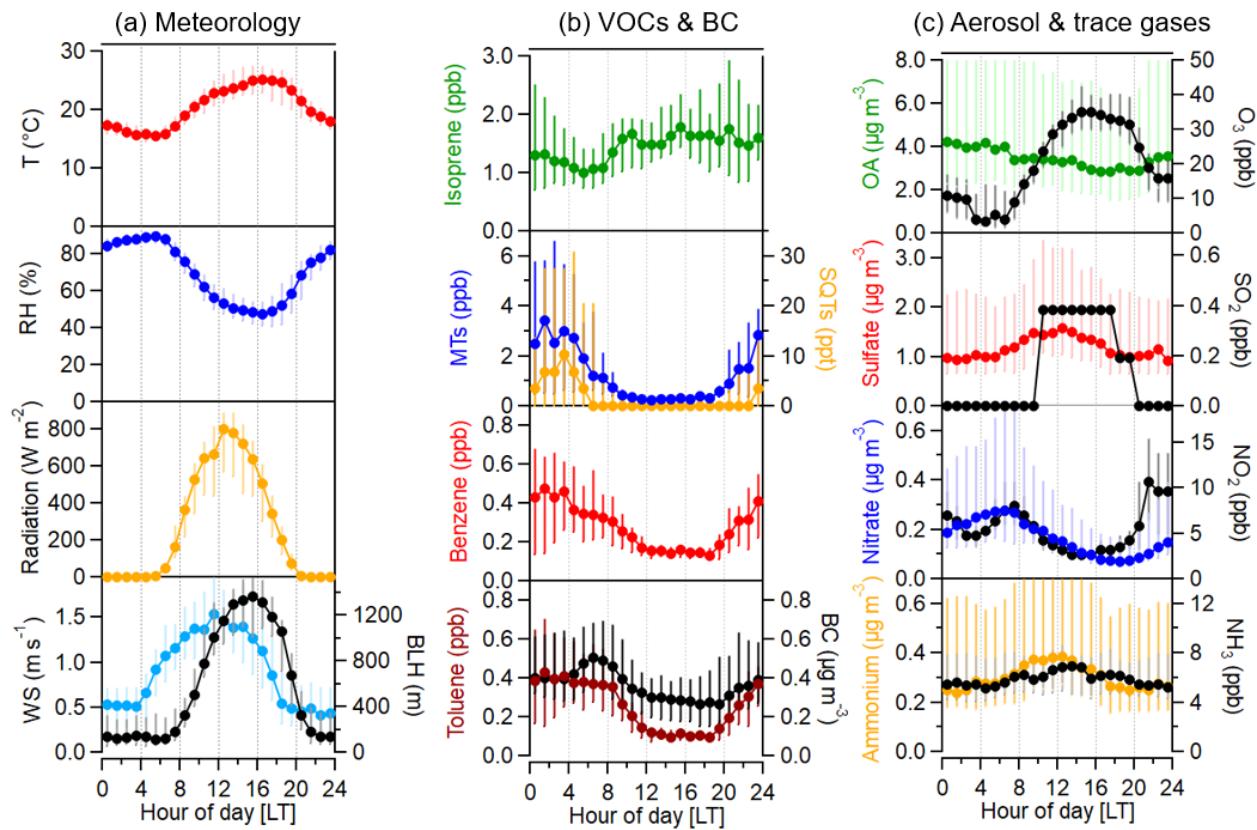
Figure S5. Diurnal variations of (a) meteorological parameters including temperature (T), relative humidity (RH), radiation, wind speeds (WS) and boundary layer height (BLH); (b) BC and VOCs including isoprene, monoterpenes (MTs), sesquiterpenes (SQTs), benzene, toluene; (c) aerosol species and trace gases including OA, sulfate, nitrate, ammonium, O_3, SO_2, NO_2 and NH_3 during the entire campaign. All data are shown in medians with the whiskers of 25th and 75th percentiles.
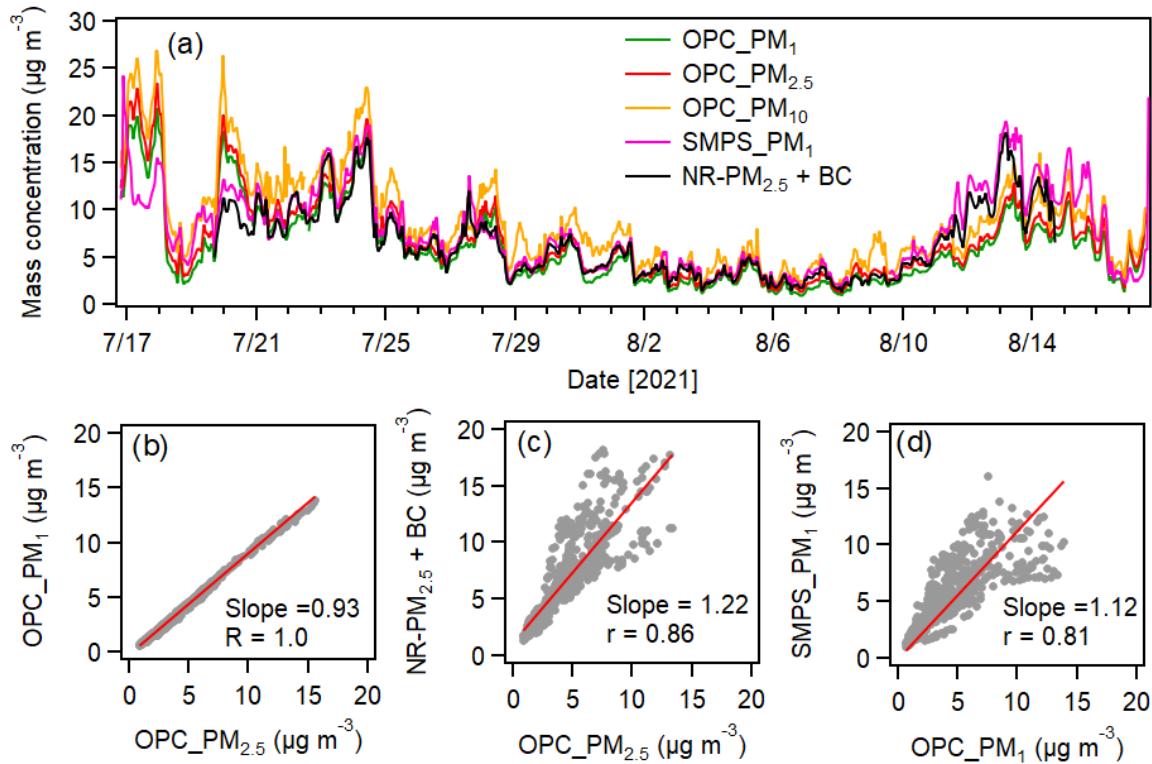
Figure S6. (a) Time series of PM_1, $PM_{2.5}$, PM_{10} measured by the OPC, PM_1 calculated from SMPS measurement (assumed density of 1.4 g cm^{-3}), and NR-$PM_{2.5}$ measured by the AMS plus BC measured by the AE33. (c-d) scatter plots between OPC_PM_1 vs. OPC_$PM_{2.5}$, OPC_$PM_{2.5}$ vs. NR-$PM_{2.5}$ plus BC, OPC_PM_1 vs. SMPS_PM_1 during the entire measurement period.
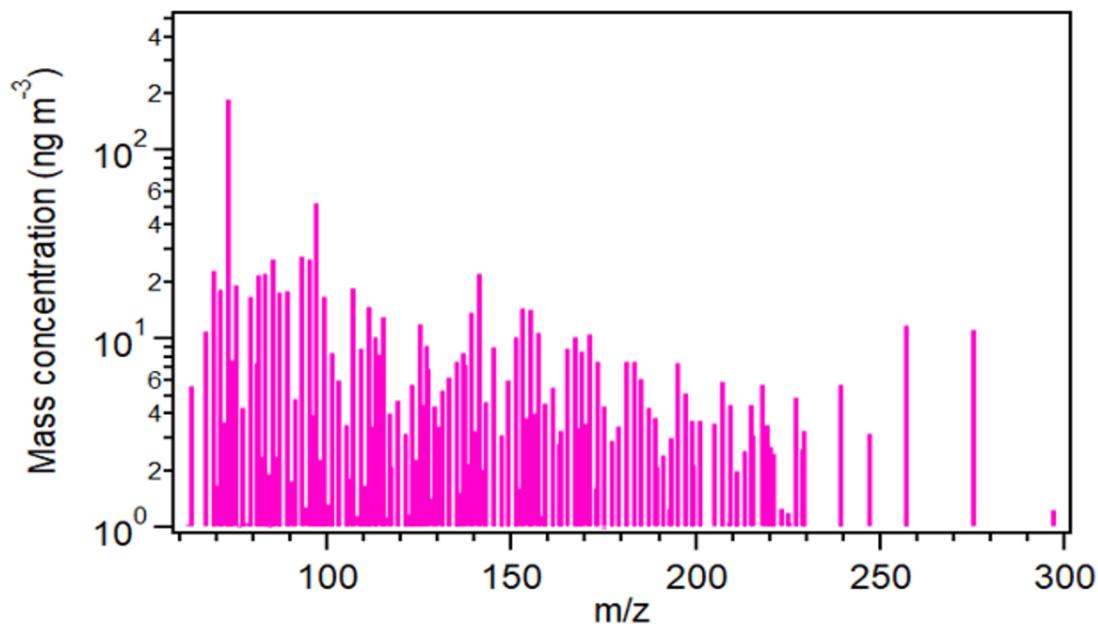
Figure S7. Median mass spectra of OA measured by the CHARON-PTR-MS

Figure S8. Key diagnostic plots for 5-factor PMF solution of PTR-measured VOCs: (a) $Q/Q_{expected}$ as a function of number of factors (P); (b) $Q/Q_{expected}$ as a function of f_{Peak};(c)) the box and whiskers plot showing the distributions of scaled residuals for each m/z; (d) time series of the measured organic mass and the reconstructed organic mass and (e) time series of variations of the residual values (= measured-reconstructed) of the fit.
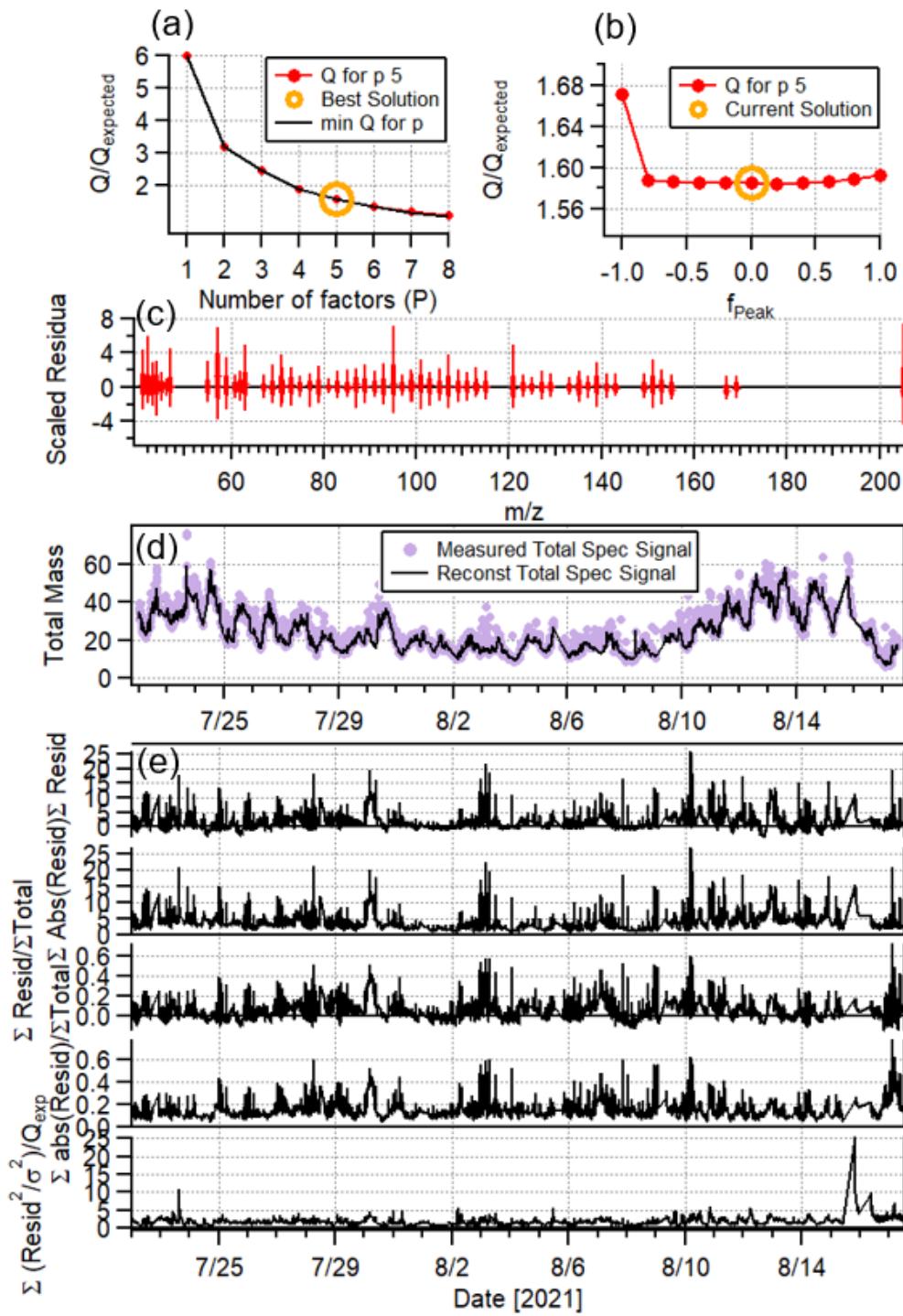
Figure S9. Key diagnostic plots for 5-factor PMF solution of AMS-measured OA: (a) $Q/Q_{expected}$ as a function of number of factors (P); (b) $Q/Q_{expected}$ as a function of f_{Peak};(c)) the box and whiskers plot showing the distributions of scaled residuals for each m/z; (d) time series of the measured organic mass and the reconstructed organic mass and (e) time series of variations of the residual values (= measured-reconstructed) of the fit.
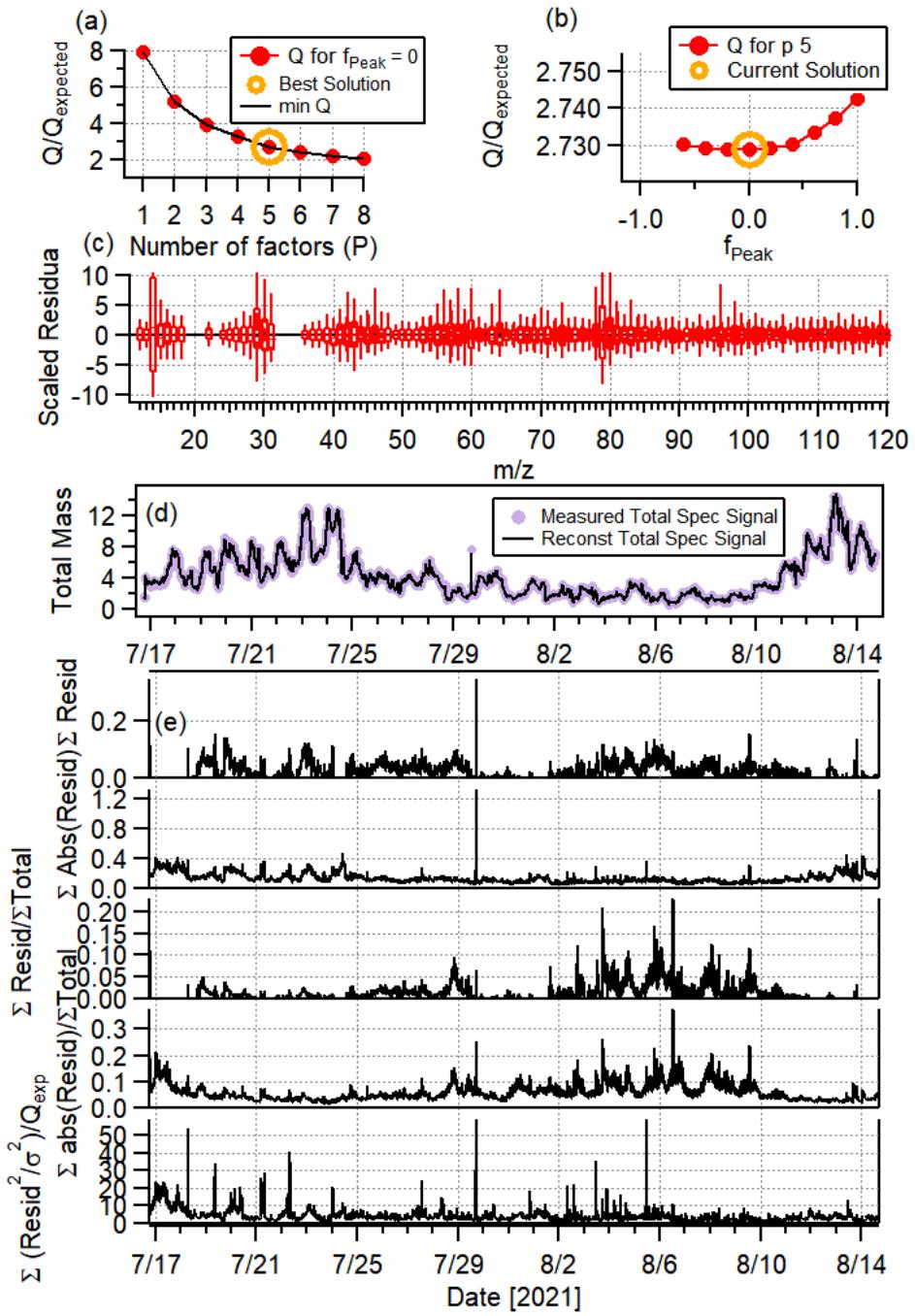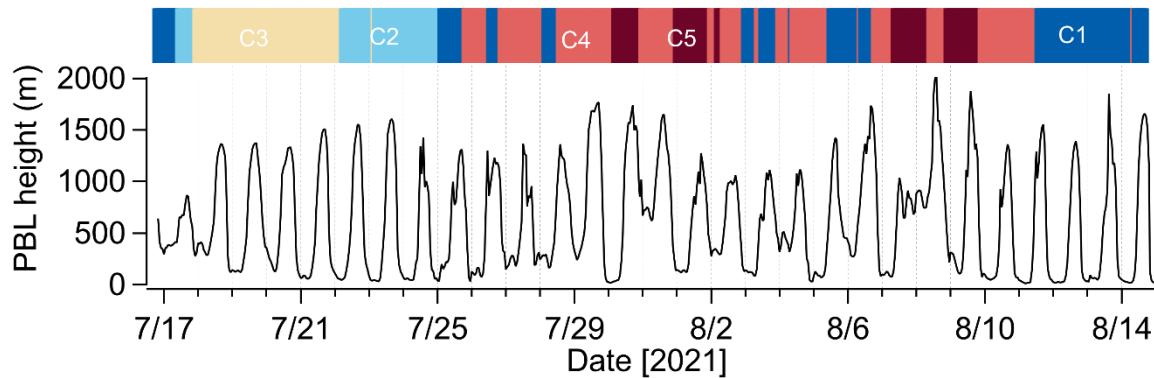
Figure S10. Time series of planetary boundary layer (PBL) height obtained from ERA5 reanalysis data over the entire campaign. The top shows the origins of five air mass clusters.

Figure S11. Time series of organic nitrate calculated from the AMS based on the method of NO_2^+/NO^+ and three organic nitrate molecules ($C_5H_7O_7N$, $C_{10}H_{15}O_8N$ and $C_{15}H_{23}O_8N$) detected by FIGAERO-CIMS related with the oxidation of isoprene, monoterpenes, sesquiterpenes respectively.

Table S1 Instruments installed in the measurement room.

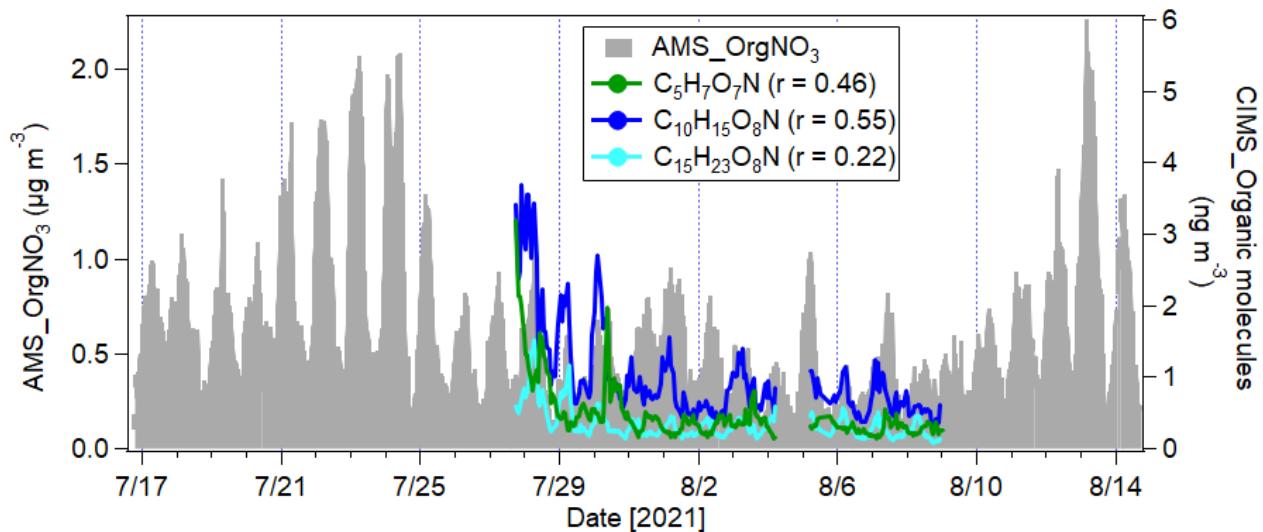| Measured parameters	Instrument	Data period	
		Starting	Ending
Meteorological parameters	WS700 (Lufft GmbH)	7/16/2021	8/17/2021
NO_2 (data missing)	AS32M (Environment SA)	7/16/2021	8/17/2021
O_3 (data missing)	O341M (Environment SA)	7/16/2021	8/17/2021
NH_3	G2103 (Picarro Inc.)	7/16/2021	8/17/2021
PM_1, $PM_{2.5}$, PM_{10} mass	OPC FIDAS200 (Palas GmbH)	7/16/2021	8/17/2021
Particle size (10–410 nm, d_m)	NanoScan-SMPS3910 (TSI Inc.)	7/16/2021	8/17/2021
Particle size (13.6-763.5 nm, d_m)	SMPS (TSI Inc.)	7/16/2021	8/17/2021
Particle number concentration	CPC3789 (TSI Inc.)	7/23/2021	8/17/2021
Black carbon	AE33 (Magee Scientific)	7/19/2021	8/17/2021
Particle mass concentration	AMS (Aerodyne Research Inc.)	7/16/2021	8/14/2021
VOCs/oxygenated VOCs	CHARON-PTR-MS (Ionicon Analytik GmbH)	7/23/2021	8/17/2021
Semi-volatile aerosol particles	CHARON-PTR-MS (Ionicon Analytik GmbH)	7/23/2021	8/17/2021
Oxygenated organic molecules	FIGAERO-CIMS (Aerodyne Research Inc.)	7/27/2021	8/09/2021

Table S2 List of VOC ions and average mixing ratios with standard deviation (Std) as well as measurement detection limit (MDL) included in the PMF analysis.

m/z	Formula	Tentative assignment	Ave (ppb)	Std (ppb)	MDL (ppb)
41.04	$C_3H_5^+$	alkyl fragment	3.078	1.752	0.1505
42.03	$C_2H_4N^+$	acetonitrile	0.361	0.413	0.0117
43.02	$C_2H_3O^+$	acetic acid fragment	5.791	3.718	0.2686
43.05	$C_3H_7^+$	propene + fragment	0.402	0.251	0.0414
44.01	CH_2NO^+	isocyanic acid	0.140	0.085	0.0103
44.05	$C_2H_5N^+$	formamide	0.096	0.042	0.0082
45.03	$C_2H_5O^+$	acetaldehyde	1.754	0.951	0.1282
46.03	CH_4NO^+	formamide	0.067	0.028	0.0054
47.01	$CH_3O_2^+$	formic acid	1.011	0.732	0.0516
47.05	$C_2H_7O^+$	ethanol	0.071	0.117	0.0006
55.02	$C_3H_3O^+$	fragment	0.084	0.053	0.0066
55.05	$C_4H_7H^+$	fragment	0.649	0.299	0.0642
57.03	$C_3H_5O^+$	acrolein	0.322	0.335	0.0177
57.07	$C_4H_9^+$	fragment	0.629	0.712	0.0331
59.05	$C_3H_7O^+$	acetone	3.828	1.621	0.1250
61.03	$C_2H_5O_2^+$	acetic acid	1.258	0.819	0.0547
62.02	$CH_4NO_2^+$	nitromethane	0.035	0.018	0.0017
63.03	$C_2H_7S^+$	dimethyl sulfide	0.035	0.018	0.0015
63.04	$C_2H_7O_2^+$	ethylene glycol	0.014	0.007	0.0014
67.05	$C_5H_7H^+$	fragment	0.166	0.093	0.0131
69.03	$C_4H_5O^+$	furan	0.084	0.038	0.0055
69.07	$C_5H_9^+$	Isoprene	0.242	0.144	0.0280
71.01	$C_3H_3O_2^+$	unknown	0.060	0.027	0.0037
71.05	$C_4H_7O^+$	methyl vinyl ketone + methacrolein	0.204	0.134	0.0092
71.09	$C_5H_{11}^+$	pentenes	0.044	0.020	0.0095
73.03	$C_3H_5O_2^+$	methylglyoxal/acrylic acid	0.171	0.063	0.0197
73.06	$C_4H_9O^+$	methyl ethyl ketone/butanals	0.152	0.085	0.0052
75.04	$C_3H_7O_2^+$	propanonic acid/hydroxyacetone	0.181	0.120	0.0091
77.02	$C_2H_5O_3^+$	glycolic acid	0.038	0.015	0.0046
79.05	$C_6H_7^+$	benzene	0.303	0.227	0.0123
81.07	$C_6H_9^+$	fragment of monoterpenes	1.060	1.420	0.0192
83.05	$C_5H_7O^+$	methylfuran	0.163	0.092	0.0080
83.09	$C_6H_{11}^+$	fragments of hexenol/hexanal	0.058	0.036	0.0110
85.03	$C_4H_5O_2^+$	furanone	0.096	0.054	0.0059
85.06	$C_5H_9O^+$	cyclopentanone	0.066	0.039	0.0037
85.10	$C_6H_{13}^+$	methylcyclopentane	0.014	0.008	0.0042
87.04	$C_4H_7O_2^+$	2,3-butanedione	0.158	0.082	0.0099
87.08	$C_5H_{11}O^+$	2-pentanone	0.015	0.009	0.0008
89.02	$C_3H_5O_3^+$	butyric acid	0.014	0.005	0.0008
89.06	$C_4H_9O_2^+$	methyl propanoate	0.016	0.012	0.0036
91.05	$C_7H_7^+$	unknown	0.102	0.081	0.0063

93.07	$C_7H_9^+$	toluene	0.282	0.219	0.0126
95.01	$C_5H_3O_2^+$	unknown	0.041	0.053	0.0016
95.05	$C_6H_7O^+$	phenol	0.170	0.047	0.0092
95.09	$C_7H_{11}^+$	fragment of monoterpenes	0.226	0.243	0.0107
97.03	$C_5H_5O_2^+$	furfural	0.023	0.011	0.0024
97.06	$C_6H_9O^+$	2-ethylfuran/2,5-dimethylfuran	0.116	0.072	0.0054
97.10	$C_7H_{13}^+$	methylcyclohexene	0.018	0.017	0.0068
99.01	$C_4H_3O_3^+$	unknown	0.028	0.017	0.0032
99.04	$C_5H_7O_2^+$	furanone	0.082	0.050	0.0045
99.08	$C_6H_{11}O^+$	cyclohexanone	0.019	0.011	0.0011
101.02	$C_4H_5O_3^+$	pentanedione	0.023	0.012	0.0019
101.06	$C_5H_9O_2^+$	C5-hydroxycarbonyl (ISOPOOH conversion product)	0.182	0.139	0.0083
103.04	$C_4H_7O_3^+$	acetic anhydride	0.012	0.007	0.0013
105.07	$C_8H_9^+$	styrene	0.033	0.028	0.0031
107.09	$C_8H_{11}^+$	C_8 aromatics (xylenes)	0.195	0.145	0.0062
109.03	$C_6H_5O_2^+$	unknown	0.012	0.008	0.0023
109.06	$C_7H_9O^+$	cresol/benzylalcohol	0.053	0.029	0.0020
109.10	$C_8H_{13}^+$	fragment of sesquiterpenes	0.067	0.048	0.0063
111.04	$C_6H_7O_2^+$		0.056	0.034	0.0033
111.08	$C_7H_{11}O^+$	heptadienal	0.048	0.029	0.0025
113.02	$C_5H_5O_3^+$	furoic acid	0.031	0.020	0.0019
113.06	$C_6H_9O_2^+$	hexendione	0.041	0.026	0.0019
115.04	$C_5H_7O_3^+$	pentanetrione	0.016	0.008	0.0011
115.08	$C_6H_{11}O_2^+$	2,5-hexanedione/ethyl-2-butenoate	0.042	0.030	0.0025
121.10	$C_9H_{13}^+$	C_9 aromatics (trimethylbenzene)	0.084	0.068	0.0037
123.08	$C_8H_{11}O^+$	unknown	0.022	0.014	0.0013
123.12	$C_9H_{15}^+$	fragment of sesquiterpenes	0.034	0.028	0.0032
125.06	$C_7H_9O_2^+$	guaiacol + dihydroxy toluene	0.024	0.015	0.0018
125.10	$C_8H_{13}O^+$	unknown	0.026	0.016	0.0019
127.04	$C_6H_7O_3^+$	unknown	0.015	0.009	0.0018
127.08	$C_7H_{11}O_2^+$	unknown	0.023	0.015	0.0004
127.11	$C_8H_{15}O^+$	E-2-octenal	0.003	0.002	0.0008
129.05	$C_6H_9O_3^+$	unknown	0.008	0.006	0.0016
129.09	$C_7H_{13}O_2^+$	unknown	0.016	0.010	0.0016
133.10	$C_{10}H_{13}^+$	cymenene	0.014	0.013	0.0029
135.08	$C_9H_{11}O^+$	unknown	0.006	0.006	0.0018
135.12	$C_{10}H_{15}^+$	C_{10} aromatics/p-cymene	0.038	0.036	0.0018
137.13	$C_{10}H_{17}^+$	monoterpenes	0.393	0.570	0.0035
139.08	$C_8H_{11}O_2^+$	unknown	0.021	0.014	0.0016
139.11	$C_9H_{15}O^+$	nopinone	0.023	0.018	0.0009
141.05	$C_7H_9O_3^+$	dicarbonyl epoxide	0.020	0.015	0.0033
141.09	$C_8H_{13}O_2^+$	unknown	0.018	0.012	0.0013
143.07	$C_7H_{11}O_3^+$	unknown	0.006	0.005	0.0021
143.11	$C_8H_{15}O_2^+$	Z-3-hexenyl acetate	0.008	0.005	0.0015
149.10	$C_{10}H_{13}O^+$	unknown	0.006	0.006	0.0010

m/z	Formula		Ave 1	Ave 2	Std
149.13	$C_{11}H_{17}^+$	fragment of sesquiterpene	0.004	0.003	0.0010
151.11	$C_{10}H_{15}O^+$	fragment of pinonaldehyde	0.027	0.026	0.0012
151.08	$C_9H_{11}O_2^+$	methylsalicylate	0.009	0.007	0.0015
153.09	$C_9H_{13}O_2^+$	unknown	0.008	0.005	0.0008
153.13	$C_{10}H_{17}O^+$	camphor	0.013	0.013	0.0007
155.07	$C_8H_{11}O_3^+$	unknown	0.008	0.009	0.0024
155.11	$C_9H_{15}O_2^+$	arbusculone, C_9 unsaturated esters	0.004	0.003	0.0006
167.07	$C_9H_{11}O_3^+$	unknown	0.007	0.007	0.0041
167.11	$C_{10}H_{15}O_2^+$	unknown	0.004	0.004	0.0015
169.09	$C_9H_{13}O_3^+$	unknown	0.003	0.005	0.0029
169.12	$C_{10}H_{17}O_2^+$	unknown	0.008	0.004	0.0007
205.20	$C_{15}H_{25}^+$	sesquiterpenes	0.002	0.004	0.0001

Table S3 List of organic ions in the particle phase measured by the CHARON included in the PMF analysis.

m/z	Formula	Ave (ng m^{-3})	Std (ng m^{-3})
63.04	$C_2H_7O_2^+$	7.0	4.3
65.02	$C_1H_5O_3^+$	1.4	2.2
67.05	$C_5H_7^+$	21.3	28.0
69.03	$C_4H_5O_1^+$	19.2	19.2
69.07	$C_5H_9^+$	29.1	19.0
71.05	$C_4H_7O_1^+$	27.3	25.4
73.03	$C_3H_5O_2^+$	185.7	35.7
73.07	$C_4H_9O_1^+$	2.5	2.3
75.04	$C_3H_7O_2^+$	22.3	11.2
77.04	$C_6H_5^+$	7.9	6.5
79.05	$C_6H_7^+$	20.3	19.6
81.07	$C_6H_9^+$	34.3	34.6
83.05	$C_5H_7O_1^+$	34.9	33.8
83.08	$C_6H_{11}^+$	16.2	6.7
85.03	$C_4H_5O_2^+$	47.0	49.7
85.07	$C_5H_9O_1^+$	7.7	6.9
87.04	$C_4H_7O_2^+$	22.3	14.8
87.08	$C_5H_{11}O_1^+$	1.6	0.6
89.02	$C_3H_5O_3^+$	3.0	3.3
89.06	$C_4H_9O_2^+$	21.3	10.9
91.05	$C_7H_7^+$	7.9	8.5

93.03	$C_6H_5O_1^+$	0.9	2.4
93.07	$C_7H_9^+$	38.7	33.0
95.04	$C_6H_7O_1^+$	39.3	37.7
95.08	$C_7H_{11}^+$	20.4	23.1
97.03	$C_5H_5O_2^+$	20.0	19.4
97.06	$C_6H_9O_1$	19.5	22.7
97.10	$C_7H_{13}^+$	8.3	2.7
99.04	$C_5H_7O_2^+$	29.4	31.6
99.08	$C_6H_{11}O_1^+$	4.5	4.3
99.12	$C_7H_{15}^+$	0.4	0.4
101.06	$C_5H_9O_2^+$	11.2	10.6
101.10	$C_6H_{13}O_1^+$	1.5	0.6
103.04	$C_4H_7O_3^+$	8.5	6.4
103.08	$C_5H_{11}O_2^+$	0.9	0.5
105.07	$C_8H_9^+$	5.7	6.1
107.05	$C_7H_7O_1^+$	4.8	2.3
107.08	$C_8H_{11}^+$	34.1	42.0
109.07	$C_7H_9O_1^+$	14.5	17.4
109.10	$C_8H_{13}^+$	15.7	18.9
111.05	$C_6H_7O_2^+$	26.2	27.0
111.08	$C_7H_{11}O_1^+$	7.8	7.8
111.11	$C_8H_{15}^+$	3.5	1.5
113.02	$C_5H_5O_3^+$	8.6	8.1
113.06	$C_6H_9O_2^+$	17.6	18.8
115.04	$C_5H_7O_3^+$	9.5	9.2
115.08	$C_6H_{11}O_2^+$	14.6	7.8
119.08	$C_9H_{11}^+$	7.1	6.6
121.02	$C_7H_5O_2^+$	2.1	1.8
121.07	$C_8H_9O_1^+$	4.8	4.4
121.10	$C_9H_{13}^+$	5.8	6.8
123.04	$C_7H_7O_2^+$	8.3	7.9
123.08	$C_8H_{11}O_1^+$	9.6	10.3
123.11	$C_9H_{15}^+$	6.9	9.4
125.03	$C_6H_5O_3^+$	4.7	4.7
125.06	$C_7H_9O_2^+$	20.1	21.1
125.10	$C_8H_{13}O_1^+$	4.9	5.1

125.13	$C_9H_{17}^+$	0.9	0.5
127.04	$C_6H_7O_3^+$	15.0	13.8
127.07	$C_7H_{11}O_2^+$	12.6	14.4
127.12	$C_8H_{15}O_1^+$	0.9	0.5
129.02	$C_5H_5O_4^+$	4.5	4.1
129.06	$C_6H_9O_3^+$	7.6	7.6
129.09	$C_7H_{13}O_2^+$	1.3	1.1
131.03	$C_5H_7O_4^+$	6.5	4.2
131.07	$C_6H_{11}O_3^+$	6.3	3.3
133.01	$C_4H_5O_5^+$	0.9	0.7
133.05	$C_5H_9O_4^+$	6.6	4.7
133.10	$C_{10}H_{13}^+$	8.8	7.0
135.04	$C_8H_7O_2^+$	3.7	3.4
135.08	$C_9H_{11}O_1^+$	10.1	6.5
135.11	$C_{10}H_{15}^+$	9.9	17.2
137.10	$C_9H_{13}O_1^+$	10.9	10.4
137.13	$C_{10}H_{17}^+$	0.2	0.3
139.04	$C_7H_7O_3^+$	18.3	22.3
139.12	$C_9H_{15}O_1^+$	0.9	0.9
141.06	$C_7H_9O_3^+$	39.4	42.1
141.13	$C_9H_{17}O_1^+$	0.5	0.7
143.03	$C_6H_7O_4^+$	4.5	4.0
143.07	$C_7H_{11}O_3^+$	8.1	7.9
143.11	$C_8H_{15}O_2^+$	1.3	1.3
145.05	$C_6H_9O_4^+$	16.3	16.1
147.08	$C_{10}H_{11}O_1^+$	4.6	4.1
149.03	$C_8H_5O_3^+$	1.5	1.7
149.06	$C_9H_9O_2^+$	6.8	5.9
151.08	$C_9H_{11}O_2^+$	15.1	12.3
151.11	$C_{10}H_{15}O_1^+$	11.2	13.2
153.05	$C_4H_9O_6^+$	9.2	9.6
153.09	$C_9H_{13}O_2^+$	24.4	26.7
153.13	$C_{10}H_{17}O_1^+$	2.0	4.3
155.07	$C_8H_{11}O_3^+$	24.5	23.3
155.10	$C_9H_{15}O_2^+$	0.8	1.5
157.05	$C_7H_9O_4^+$	20.0	21.3

159.06	$C_7H_{11}O_4^+$	7.7	6.9
163.05	$C_{13}H_7^+$	4.3	3.7
163.08	$C_{10}H_{11}O_2^+$	5.2	5.2
163.13	$C_8H_{19}O_3^+$	1.3	0.8
165.02	$C_8H_5O_4^+$	1.1	0.9
165.09	$C_{10}H_{13}O_2^+$	14.1	14.4
167.03	$C_8H_7O_4^+$	0.8	0.9
167.07	$C_9H_{11}O_3^+$	16.1	14.6
167.11	$C_{10}H_{15}O_2^+$	6.0	7.2
169.05	$C_8H_9O_4^+$	8.1	7.2
169.09	$C_9H_{13}O_3^+$	15.0	16.5
171.07	$C_8H_{11}O_4^+$	19.2	19.3
171.17	$C_{11}H_{23}O_1^+$	2.0	1.1
173.04	$C_7H_9O_5^+$	2.8	2.7
175.07	$C_{11}H_{11}O_2^+$	6.7	5.7
177.05	$C_6H_9O_6^+$	3.2	2.7
179.07	$C_{10}H_{11}O_3^+$	4.8	3.7
179.09	$C_{14}H_{11}^+$	4.4	3.4
181.09	$C_{10}H_{13}O_3^+$	12.7	13.1
183.10	$C_{10}H_{15}O_3^+$	10.1	11.2
183.17	$C_{12}H_{23}O_1^+$	0.8	0.7
185.01	$C_7H_5O_6^+$	0.9	0.7
185.08	$C_9H_{13}O_4^+$	10.9	10.7
185.16	$C_{11}H_{21}O_2^+$	1.8	0.7
187.06	$C_8H_{11}O_5^+$	5.9	5.5
187.17	$C_{11}H_{23}O_2^+$	0.5	0.3
189.06	$C_{15}H_9^+$	5.9	5.1
191.05	$C_7H_{11}O_6^+$	3.3	2.4
191.15	$C_{13}H_{19}O_1^+$	1.8	1.4
193.07	$C_7H_{13}O_6^+$	4.3	3.4
193.17	$C_{13}H_{21}O_1^+$	1.2	1.1
195.12	$C_8H_{19}O_5^+$	9.9	6.2
197.09	$C_{10}H_{13}O_4^+$	9.0	8.9
197.19	$C_{13}H_{25}O_1^+$	0.8	0.5
199.05	$C_9H_{11}O_5^+$	3.2	2.6
199.09	$C_{10}H_{15}O_4^+$	7.4	8.4

201.07	$C_{16}H_9^+$	6.5	6.6
201.19	$C_{12}H_{25}O_2^+$	4.0	1.9
205.12	$C_{13}H_{17}O_2^+$	4.9	3.4
205.20	$C_{15}H_{25}^+$	0.5	0.4
207.03	$C_{10}H_7O_5^+$	1.9	1.6
207.15	$C_{13}H_{19}O_2^+$	7.4	4.6
209.01	$C_9H_5O_6^+$	1.4	1.0
211.09	$C_7H_{15}O_7^+$	3.3	3.2
211.20	$C_{14}H_{27}O_1^+$	1.6	0.8
213.08	$C_{10}H_{13}O_5^+$	4.6	4.4
219.06	$C_8H_{11}O_7^+$	2.1	1.5
219.18	$C_{15}H_{23}O_1^+$	4.0	2.0
221.11	$C_9H_{17}O_6^+$	3.3	2.5
223.07	$C_{15}H_{11}O_2^+$	2.9	3.5
225.06	$C_{14}H_9O_3^+$	2.2	2.4
225.22	$C_{15}H_{29}O_1^+$	1.4	0.9
227.21	$C_{14}H_{27}O_2^+$	5.2	1.8
229.10	$C_{18}H_{13}^+$	2.9	2.5
229.22	$C_{14}H_{29}O_2^+$	3.5	1.7
239.11	$C_{16}H_{15}O_2^+$	6.4	3.6
247.10	$C_{14}H_{15}O_4^+$	1.3	1.0
247.23	$C_{14}H_{31}O_3^+$	3.3	1.5
257.25	$C_{16}H_{33}O_2^+$	13.5	6.8
275.26	$C_{16}H_{35}O_3^+$	12.8	6.7
299.07	$C_{20}H_{11}O_3^+$	0.5	0.6

References

Bosque, R. and Sales, J.: Polarizabilities of Solvents from the Chemical Composition, Journal of Chemical Information and Computer Sciences, 42, 1154-1163, 10.1021/ci025528x, 2002.

Chen, Y., Takeuchi, M., Nah, T., Xu, L., Canagaratna, M. R., Stark, H., Baumann, K., Canonaco, F., Prévôt, A. S. H., Huey, L. G., Weber, R. J., and Ng, N. L.: Chemical characterization of secondary organic aerosol at a rural site in the southeastern US: insights from simultaneous high-resolution time-of-flight aerosol mass spectrometer (HR-ToF-AMS) and FIGAERO chemical ionization mass spectrometer (CIMS) measurements, Atmos. Chem. Phys., 20, 8421-8440, 10.5194/acp-20-8421-2020, 2020.

Farmer, D. K., Matsunaga, A., Docherty, K. S., Surratt, J. D., Seinfeld, J. H., Ziemann, P. J., and Jimenez, J. L.: Response of an aerosol mass spectrometer to organonitrates and organosulfates and implications for atmospheric chemistry, P. Natl. Acad. Sci. USA, 107, 6670-6675, 2010.

Gao, L., Song, J., Mohr, C., Huang, W., Vallon, M., Jiang, F., Leisner, T., and Saathoff, H.: Kinetics, SOA yields, and chemical composition of secondary organic aerosol from β-caryophyllene ozonolysis with and without nitrogen oxides between 213 and 313 K, Atmos. Chem. Phys., 22, 6001-6020, 10.5194/acp-22-6001-2022, 2022.

Huang, W., Saathoff, H., Shen, X., Ramisetty, R., Leisner, T., and Mohr, C.: Chemical Characterization of Highly Functionalized Organonitrates Contributing to Night-Time Organic Aerosol Mass Loadings and Particle Growth, Environ. Sci. Technol., 53, 1165-1174, 10.1021/acs.est.8b05826, 2019.

Kiendler-Scharr, A., Mensah, A. A., Friese, E., Topping, D., Nemitz, E., Prevot, A. S. H., Aijala, M., Allan, J., Canonaco, F., Canagaratna, M., Carbone, S., Crippa, M., Dall Osto, M., Day, D. A., De Carlo, P., Di Marco, C. F., Elbern, H., Eriksson, A., Freney, E., Hao, L., Herrmann, H., Hildebrandt, L., Hillamo, R., Jimenez, J. L., Laaksonen, A., McFiggans, G., Mohr, C., O'Dowd, C., Otjes, R., Ovadnevaite, J., Pandis, S. N., Poulain, L., Schlag, P., Sellegri, K., Swietlicki, E., Tiitta, P., Vermeulen, A., Wahner, A., Worsnop, D., and Wu, H. C.: Ubiquity of organic nitrates from nighttime chemistry in the European submicron aerosol, Geophys. Res. Lett., 43, 7735-7744, 2016.

Muller, M., Eicher, P., D'Anna, B., Tan, W., and Wisthaler, A.: Direct Sampling and Analysis of Atmospheric Particulate Organic Matter by Proton-Transfer-Reaction Mass Spectrometry, Analytical Chemistry, 89, 10889-10897, 10.1021/acs.analchem.7b02582, 2017.

Pagonis, D., Sekimoto, K., and de Gouw, J.: A Library of Proton-Transfer Reactions of H3O+ Ions Used for Trace Gas Detection, Journal of the American Society for Mass Spectrometry, 30, 1330-1335, 10.1007/s13361-019-02209-3, 2019.

Piel, F., Müller, M., Winkler, K., Skytte af Sätra, J., and Wisthaler, A.: Introducing the extended volatility range proton-transfer-reaction mass spectrometer (EVR PTR-MS), Atmos. Meas. Tech., 14, 1355-1363, 10.5194/amt-14-1355-2021, 2021.

Su, T.: Trajectory calculations of ion–polar molecule capture rate constants at low temperatures, The Journal of Chemical Physics, 88, 4102-4103, 10.1063/1.453817, 1988.

Xu, L., Suresh, S., Guo, H., Weber, R. J., and Ng, N. L.: Aerosol characterization over the southeastern United States using high-resolution aerosol mass spectrometry: spatial and seasonal variation of aerosol composition and sources with a focus on organic nitrates, Atmos. Chem. Phys., 15, 7307-7336, 10.5194/acp-15-7307-2015, 2015.

Yáñez-Serrano, A. M., Filella, I., Llusià, J., Gargallo-Garriga, A., Granda, V., Bourtsoukidis, E., Williams, J., Seco, R., Cappellin, L., Werner, C., de Gouw, J., and Peñuelas, J.: GLOVOCS - Master compound assignment guide for proton transfer reaction mass spectrometry users, Atmos. Environ., 244, 117929, https://doi.org/10.1016/j.atmosenv.2020.117929, 2021.

Yuan, B., Koss, A. R., Warneke, C., Coggon, M., Sekimoto, K., and de Gouw, J. A.: Proton-Transfer-Reaction Mass Spectrometry: Applications in Atmospheric Sciences, Chemical Reviews, 117, 13187-13229, 10.1021/acs.chemrev.7b00325, 2017.